J. Fluid Mech. (1987), *vol.* 176, *pp.* 333–356
Printed in Great Britain

Influence of surface roughness on the transition from regular to Mach reflection in pseudo-steady flows

By G. BEN-DOR, G. MAZOR,
Department of Mechanical Engineering, Ben-Gurion University of the Negev, Beer Sheva, Israel

K. TAKAYAMA
Institute of High Speed Mechanics, Tohoku University, Sendai Japan

AND O. IGRA
Department of Mechanical Engineering, Ben-Gurion University of the Negev, Beer Sheva, Israel

(Received 18 April 1986)

The effect of surface roughness on the transition from regular (RR) to Mach reflection (MR) over straight wedges in pseudo-steady flows was investigated both experimentally and analytically. A model for predicting the RR$\rightleftarrows$MR transition in the (M_1, θ_w)-plane was developed (M_1 is the incident shock wave Mach number and θ_w is the reflecting wedge angle). Its validity was checked against experimental results. Since the experimental results are limited to the ranges $1 < M_1 < 2$ and surface roughness heights of $0 < \epsilon \leqslant 0.2$ cm, the proposed model is applicable to these ranges only. In the proposed model (the boundary-layer displacement-thickness model), the RR$\rightleftarrows$MR transition is related to the boundary-layer thickness which in turn depends on the surface roughness.

1. Introduction

When a planar incident normal shock wave encounters a sharp corner in a shock tube, four different types of reflection can occur depending on the incident-shock-wave Mach number M_1 and the wedge angle θ_w. They are: (i) regular reflection, RR; (ii) single-Mach reflection, SMR; (iii) complex-Mach reflection, CMR; and (iv) double-Mach reflection, DMR. The latter three types are usually termed Mach reflections, MR.

The RR$\rightleftarrows$MR transition criterion in pseudo-steady flows (the 'detachment criterion') was first introduced by von Neumann (1943). In developing this criterion von Neumann assumed that (i) the flow is ideal, i.e. $\mu = 0$ and $k = 0$ (μ is the dynamic viscosity and k the thermal conductivity); (ii) the flow is two-dimensional; and (iii) the flow is self-similar and hence pseudo-steady.

As shown by Ben-Dor & Glass (1979), the detachment criterion can be expressed as follows:

$$\theta_1 - \theta_{2m} = 0, \tag{1}$$

where θ_1 is the flow deflection through the incident shock wave i, and θ_{2m} is the maximum possible flow deflection through the reflected shock wave r. This formu-

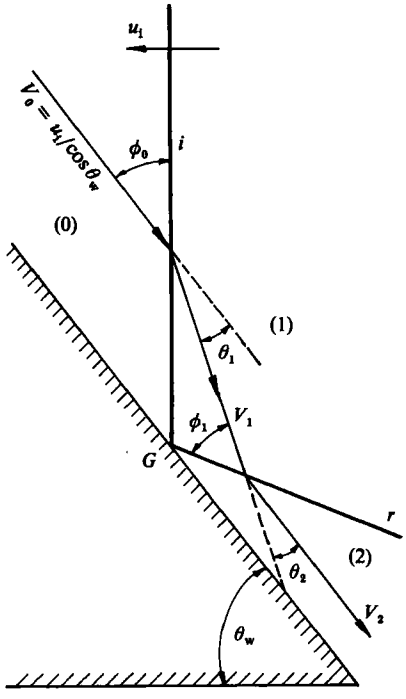

FIGURE 1. The wave configuration of a regular reflection: i, incident shock wave; r, reflected shock wave; G, reflection point; u_i, velocity of the incident shock wave in the laboratory frame of reference; V, velocity of the flow in a frame of reference moving with point G; θ_w, reflecting wedge angle; ϕ, angle of incidence; θ, flow deflection angle; (0)–(2), thermodynamic flow states.

lation is based on the fact that when the frame of reference is attached to the reflection point G (figure 1) the flow ahead of the incident shock wave i, which now moves parallel to the wedge surface at supersonic velocity $V_0 = u_i/\cos\theta_w$ (u_i is the incident shock wave velocity), is deflected towards the solid wedge surface by an angle θ_1. In order to negotiate the solid surface it must experience a redeflection while crossing the reflected shock wave r to become parallel again to the wedge surface. When the angle exceeds the maximum deflection angle θ_{2m}, the regular reflection becomes theoretically impossible. Consequently (i) represents the 'detachment' criterion of von Neumann. However, the experimental findings of Smith (1945), Taub (1947), Bleakney & Taub (1949), Fletcher (1950), White (1951), Law (1970), Henderson & Lozzi (1975), Hornung & Taylor (1982), Ben-Dor & Glass (1979) and Henderson & Woolmington (1983) indicate that the RR exists beyond the predicted theoretical limit of the 'detachment' criterion.

Since the von Neumann paradox was first noticed (see von Neumann 1963) many scientists such as Ben-Dor & Glass (1979), Hornung & Taylor (1982), Henderson & Woolmington (1983) directed their efforts at resolving this paradox. Probably the most promising approach was the one suggested by Hornung & Taylor (1982) who argued that the reason for the existence of the von Neumann paradox is the fact that the transition line was derived by solving the inviscid-flow conservation equations whereas the actual flow is viscous. Consequently, they concluded that by accounting for viscous effects the von Neumann paradox could be resolved. In their work they accounted for the viscous effects by applying the boundary-layer displacement-thickness concept. Their obtained results justified their approach.

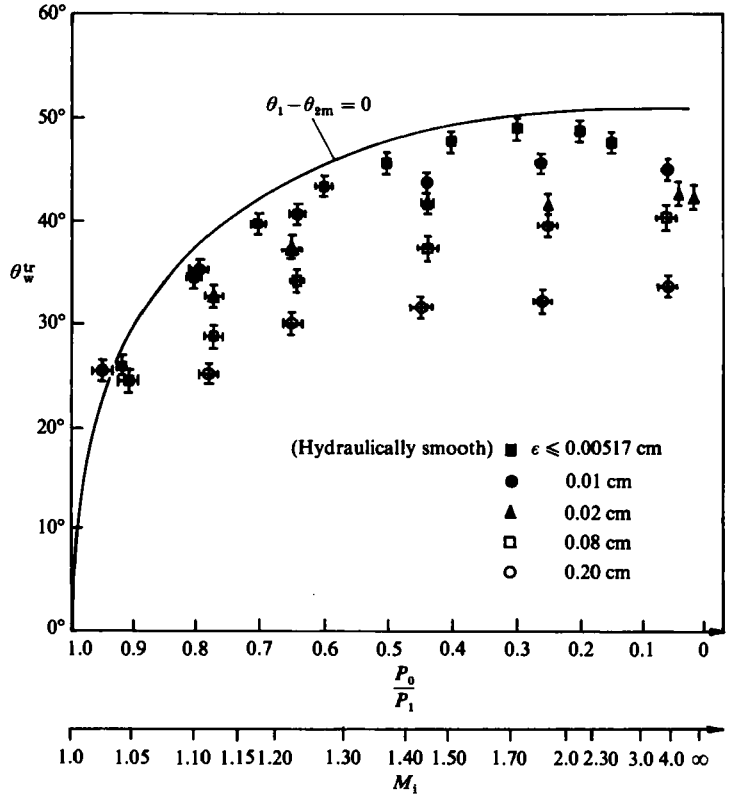

FIGURE 2. Experimental results of the RR ⇄ MR transition over rough wedges, ϵ, roughness height; the solid line is the 'detachment' transition line of von Neumann (1943).

Takayama, Ben-Dor & Gotoh (1981) presented experimental results regarding the RR ⇄ MR transition over rough surfaces. Their results are reproduced in figure 2. The difference between the actual transition and that predicted by the detachment criterion (solid line) is quite clear. This difference increases as the roughness height increases. For example, at $M_1 = 4$ and $\epsilon = 0.2$ cm, the actual wedge angle at which the RR ⇄ MR transition occurs is about 20° lower than that predicted by the 'detachment' criterion.

The fact that the surface roughness has such a meaningful influence on the transition wedge angle on one hand, and the fact that shock reflections, in nature, occur over rough surfaces on the other hand, has led to the recognition that understanding the reflection process over rough surfaces is of great importance. Consequently, a model capable of predicting the RR ⇄ MR transition over rough surfaces was sought.

Based on the foregoing discussion, the RR ⇄ MR transition process was investigated both experimentally and analytically. Since Hornung & Taylor (1982) were able to explain the von Neumann paradox by including viscous effects in their solution of the flow field, it was decided to adopt their approach for predicting the RR ⇄ MR transition over rough surfaces as well.

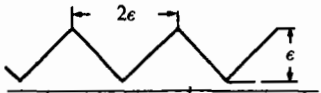

ε[cm]	model
0.01	I
0.02	II
0.08	III
0.2	IV

(*a*)

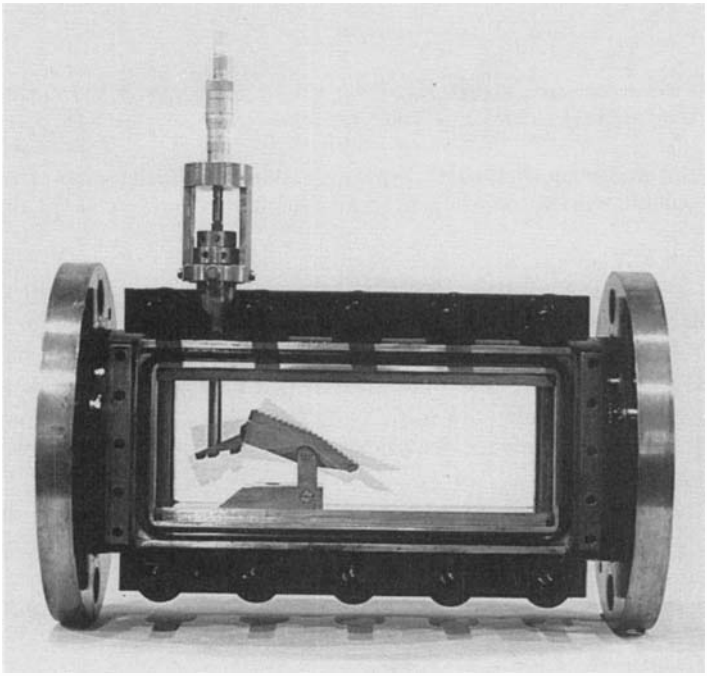

(*b*)

FIGURE 3. (*a*) Schematic illustration of the type of roughness used in the experimental study. (*b*) The test section and the adjustable wedge model.

2. Experimental results

The experimental results reported here were obtained using the 40×80 mm shock tube of the Institute of High Speed Mechanics, Tohoku University, Sendai, Japan. The 'saw-tooth' roughness imposed on the tested wedge models is illustrated in figure 3(*a*). For the first set of experiments four models (each 4 cm long) with roughness of $\epsilon = 0.01, 0.02, 0.08$ and 0.2 cm were prepared. The wedge angle of the models could be adjusted from outside the shock-tube test section as shown in figure 3(*b*). The experimental study covered the range $1 < M_1 \leqslant 4$.

The shock-wave velocity was measured using Kistler 606 pressure transducers, an Iwatsu UC7641 digital counter and an Iwatsu DM901 recorder. The pressure transducers were mounted 120 mm apart just ahead of the test section. The attenuation of the incident shock wave was found to be negligibly small.

The gas was pure nitrogen. The initial pressures were in the range $3 < P_0 \leqslant 50$ Torr. For all the experiments the initial temperature was about $T_0 = 300$ K. For the investigated range of shock-wave Mach numbers ($1 < M_1 < 4$) the nitrogen can be assumed to behave as a perfect gas.

An optical diagnostic (shadowgraph) was used for studying the pseudo-steady reflection phenomenon. A pulsed ruby laser (6493 Å) was used as a light source.

The RR $\rightleftarrows$ MR transition angle was determined in the following way. For a given value of the incident-shock-wave Mach number M_1 the wedge angle θ_w was gradually increased until an RR was obtained. Then, the value of the triple-point trajectory angle χ (deduced from the shadowgraphs) was plotted in the (χ, θ_w)-plane. The experimental results were then linearly extrapolated to $\chi = 0$. The wedge angle at this point was chosen as the transition wedge angle θ_w^{tr}. This procedure yields values of θ_w^{tr} to an accuracy of $\pm 1°$. The above-mentioned procedure was repeated for $M_1 = 1.04$, 1.12, 1.21, 1.44, 1.96, 3.58, 3.77 and 3.89. The experimental results obtained for the four different models, as well as the results obtained for a 'smooth' model, are shown in figure 2.

It is apparent that the surface roughness ϵ has a significant influence on the RR $\rightleftarrows$ MR transition wedge angle for any given incident-shock-wave Mach number. The greater ϵ is, the smaller is the transition wedge angle θ_w^{tr}. It is of interest to note that the measured transition wedge angles over the smooth-surface model do not agree with the 'detachment' criterion (these results confirm the von Neumann paradox). Had the surface been perfectly smooth, i.e. $\epsilon = 0$, and the flow truly inviscid, the experimental results should have agreed with the 'detachment' criterion. However, since no surface is perfectly smooth, and since no flow is truly inviscid, the von Neumann paradox exists. In the following we shall refer to a 'smooth' surface as hydraulically smooth. As shown in the Appendix, a hydraulically smooth surface is one for which $\epsilon \leqslant 0.00517$ cm.

3. Analysis

As mentioned previously the aim of the present study is to develop a model capable of predicting the RR $\rightleftarrows$ MR transition over rough surfaces, i.e. a model that will shift the 'detachment' transition line (solid line in figure 2) towards the experimental results for any given roughness height ϵ.

3.1. *General assumptions*

(i) The flow is two-dimensional; (ii) the flow field can be described by the mass, momentum and energy conservation equations of inviscid flows with additional terms accounting for viscous effects; (iii) the flow is self-similar, and hence can be made pseudo-steady by applying the well-known Galilean transformation; and (iv) real-gas effects can be ignored, consequently the gas is assumed to obey the equation of state of perfect gas (i.e. $P = \rho RT$).

3.2. *The conservation equations*

The wave configuration of an RR is shown schematically in figure 1. Employing the foregoing assumptions, and attaching the frame of reference to the reflection point G (in such a way that it moves along the wedge surface together with point G) results in the following nine equations which completely describe the flow field in the vicinity of the reflection point G. Across the incident shock wave i:

continuity $$\rho_0 V_0 \sin\phi_0 = \rho_1 V_1 \sin(\phi_0 - \theta_1); \tag{2}$$

tangential momentum $$\rho_0 \tan\phi_0 = \rho_1 \tan(\phi_0 - \theta_1); \tag{3}$$

normal momentum $$P_0 + \rho_0 V_0^2 \sin^2\phi_0 = P_1 + \rho_1 V_1^2 \sin^2(\phi_0 - \theta_1); \tag{4}$$

energy $$h_0 + \tfrac{1}{2} V_0^2 \sin^2\phi_0 = h_1 + \tfrac{1}{2} V_1^2 \sin^2(\phi_0 - \theta_1). \tag{5}$$

Across the reflected shock wave r:

continuity $$\rho_1 V_1 \sin\phi_1 = \rho_2 V_2 \sin(\phi_1 - \theta_2); \tag{6}$$

tangential momentum $$\rho_1 \tan\phi_1 = \rho_2 \tan(\phi_1 - \theta_2); \tag{7}$$

normal momentum $$P_1 + \rho_1 V_1^2 \sin^2\phi_1 = P_2 + \rho_2 V_2^2 \sin^2(\phi_1 - \theta_2); \tag{8}$$

energy $$h_1 + \tfrac{1}{2} V_1^2 \sin^2\phi_1 = h_2 + \tfrac{1}{2} V_2^2 \sin^2(\phi_1 - \theta_2). \tag{9}$$

The boundary condition for the RR $\rightleftarrows$ MR transition:

$$\theta_1 - \theta_2 = \gamma. \tag{10a}$$

Recalling that at the transition from RR to MR, θ_2 reaches its maximum value, θ_{2m}, (10a) should read

$$\theta_1 - \theta_{2m} = \gamma \tag{10b}$$

or alternatively

$$1 - \frac{\theta_{2m}}{\theta_1} = \frac{\gamma}{\theta_1} = F_\gamma. \tag{10c}$$

Setting $\gamma = 0$ results in the well-known set of equations describing a regular reflection in an inviscid flow (Ben-Dor 1978). The solution of these equations, which yields the 'detachment' transition line (shown in figure 2), can be found in Ben-Dor's (1978) report. Note that $V_0 = u_i/\cos\theta_w$, $\phi_0 = 90° - \theta_w$, P_0 and T_0 are known. The enthalpy h is related to the temperature through $h = C_p T$ and the density ρ can be calculated from the equation of state for a perfect gas, i.e. $\rho = P/RT$. The definitions of ϕ_0, ϕ_1, θ_1 and θ_2 are shown in figure 1.

However, in reality no flow is perfectly inviscid. Consequently, as the flow negotiates a solid surface it develops a boundary layer inside which viscous effects are dominant and must be accounted for.

One technique of overcoming this difficulty is by 'displacing' the solid boundary over which the fluid flows and still using the conservation equations for an inviscid

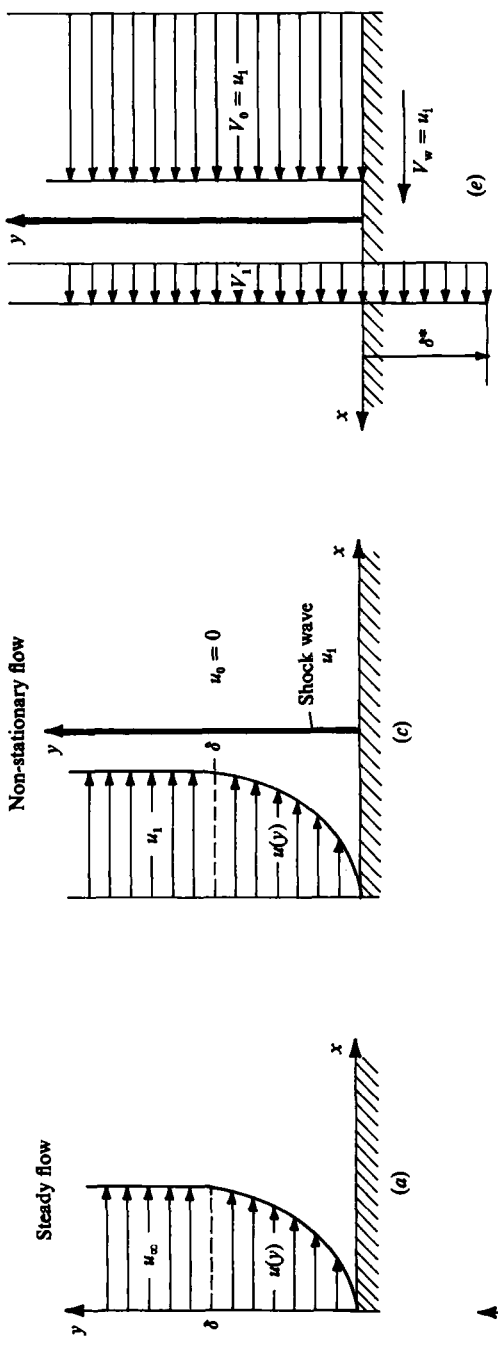

FIGURE 4. Schematic illustration of the boundary-layer displacement thickness in steady and pseudo-steady flows. (*a*) The velocity profile of a steady flow over a flat plate. At $y \geqslant \delta$, $u = u_\infty$ and at $y < \delta$, $u = u(y)$. (*b*) The velocity profile of a steady flow over the displaced boundary. At $y \geqslant \delta^*$, $u = u_\infty$. (*c*) The shock-induced-flow velocity profile over a flat plate. At $y \geqslant \delta$, $u = u_1$ and at $y < \delta$, $u = u(y)$ ahead of the shock wave $u_0 = 0$. (*d*) The Galilean transformation of the flow field shown in (*c*). At $y \geqslant \delta$, $V = V_1$ and at $y < \delta$, $V = V(y) = u_1 - u(y)$, where u_1 is the shock-wave velocity. (*e*) The velocity profile of a pseudo-steady flow over the displaced boundary. At $y \geqslant -\delta^* V = V_1$. Note in both (*d*) and (*e*) the flat plate is moving with the velocity $V_w = u_1$.

flow over the displaced wall. The procedure is shown schematically in figure 4. Figure 4(*a*) illustrates the actual velocity profile of a flow over a flat plate. At $y \geqslant \delta$ the velocity is uniform and equal to u_∞. As the flow approaches the plate surface, the velocity decreases. At $y = 0$, the flow velocity is equal to the plate velocity, which is zero for this case. Figure 4(*b*) illustrates a uniform flow of velocity u_∞ over a boundary which is displaced by δ^*. The mass flow for the two cases shown in figure 4(*a*, *b*) is identical.

The situation is somewhat different for the pseudo-steady case. Figure 4(*c*) illustrates the actual velocity profile of the flow induced by the normal shock wave which propagates from left to right at a constant speed u_i into a quiescent flow, i.e. $u_0 = 0$. At $y \geqslant \delta$ the induced flow velocity is u_1 and it reduces to zero on the plate. By considering the flow from a frame of reference attached to the shock wave, i.e. performing a Galilean transformation on the entire velocity field, the flow profile illustrated in figure 4(*d*) is obtained. At $y \geqslant \delta$ the flow velocity is $V_1 = u_i - u_1$. As the flow approaches the plate surface its velocity increases until it reaches the plate velocity u_i at $y = 0$. In order to have a uniform flow of velocity V_1 with the same mass flow as that of figure 4(*d*), the boundary has to be displaced downwards, as shown in figure 4(*e*). Thus in this case the boundary displacement thickness δ^* is negative.

Applying this technique to the regular reflection shown in figure 5(*a*) results in the regular reflection shown in figure 5(*b*). One can either solve the problem shown in figure 5(*a*) while accounting for viscous effects in regions (2) and requiring $\theta_1 - \theta_2 = 0$, or alternatively use inviscid-flow equations and solve for the displaced geometry shown in figure 5(*b*). In this case, it is clear that $\theta_1 - \theta_2 = \gamma \neq 0$. The value of γ appearing in the last expression can be obtained from the boundary displacement thickness δ^* which in turn can be obtained from the boundary-layer thickness δ. The procedure for obtaining γ is outlined in the following.

3.3. *The roughness effect on the turbulent flow*

Usually, surfaces over which fluids flow cannot be considered as perfectly smooth. Experiments have indicated that the roughness height ϵ significantly contributes to the friction coefficient f. Thus it is necessary to develop a model that will relate the friction coefficient f to the roughness height ϵ.

Blasius (in Schlichting 1962) showed experimentally that for hydraulically smooth pipes the friction coefficient f depends solely on the Reynolds number Re. Hopf (1923) found experimentally that for very rough pipes the friction coefficient f depends solely on the relative roughness ϵ/R (R is the pipe radius). Furthermore, he showed that for less rough pipes f depends on both Re and ϵ/R. These experimental findings suggested that f is controlled by the thickness of the laminar sublayer δ_L. Their conclusion was that the dominant factor in determining the value of the friction coefficient f is ϵ/δ_L. When $\epsilon < \delta_L$ (i.e. the surface roughness is completely immersed inside the laminar sublayer) the roughness has practically no effect on f, and the surface can be considered as 'hydraulically smooth'. On the other hand, for $\epsilon \gg \delta_L$ the roughness has a dominant effect on f. In such a case the friction mechanism is known as 'wave drag' (Shames 1982). It was further shown by Schlichting (1962) that for any given size of roughness, $V_* \delta_L/\nu = C_1$, where C_1 is a constant, V_* is the shear velocity and ν is the kinematic viscosity. This finding leads to the following relation:

$$\frac{\epsilon}{\delta_L} = \frac{1}{C_1} \frac{\epsilon V_*}{\nu}. \tag{11}$$

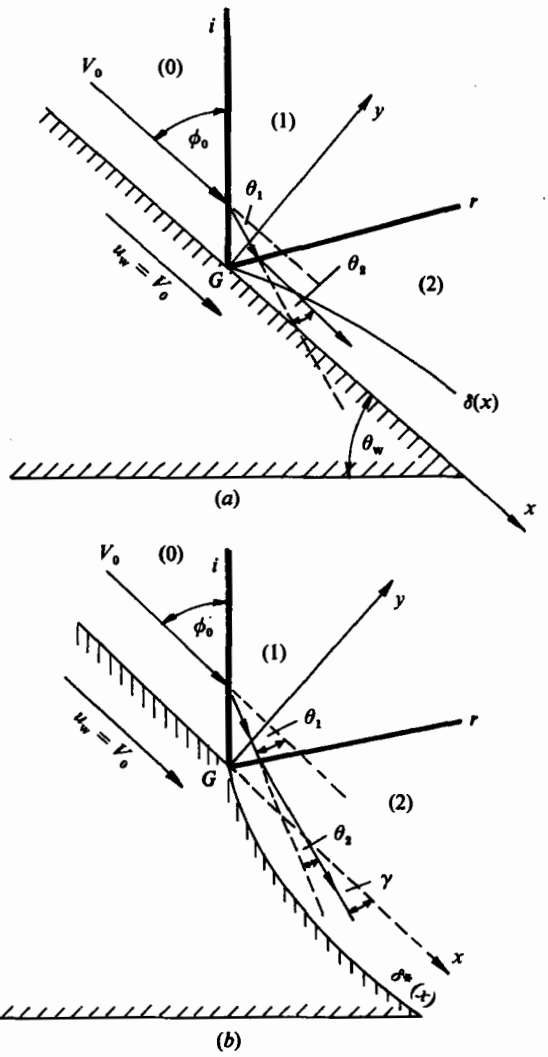

FIGURE 5. The flow field associated with a regular reflection over a wedge in a pseudo-steady flow. (*a*) Viscous flow over the real surface. Note, a boundary layer is developed in state (2). (*b*) Inviscid flow over the displaced surface.

It is clear from this relation that $\epsilon V_*/\nu$ can replace ϵ/δ_L and therefore be considered as the dominant factor in determining the value of the friction coefficient.

Based on the experimental results of Nikuradse (1933) it is a common practice to divide the turbulent flow over rough surfaces into three flow zones (Shames 1982):

(i) hydraulically smooth flow

$$\frac{\epsilon}{\delta_L} < 1 \quad \text{or} \quad \frac{\epsilon V_*}{\nu} < 5 \quad \text{where } f = f(Re);$$

(ii) frictional transition flow

$$1 < \frac{\epsilon}{\delta_L} < 15 \quad \text{or} \quad 5 < \frac{\epsilon V_*}{\nu} < 70 \quad \text{where } f = f\left(Re, \frac{\epsilon}{R}\right);$$

(iii) rough flow

$$\frac{\epsilon}{\delta_L} > 15 \quad \text{or} \quad \frac{\epsilon V_*}{\nu} > 70 \quad \text{where } f = f\left(\frac{\epsilon}{R}\right).$$

Once the turbulent character of the flow is defined it is important to correlate the roughness and the friction losses. As a basis for constructing such correlations the following logarithmic velocity distribution law is used (Shames 1982, pp. 322–324):

$$\frac{\bar{u}}{V_*} = \frac{1}{\alpha}\left[\ln\frac{V_* y}{\nu} - \ln\beta\right], \tag{12}$$

where $\bar{u}$ is the time-averaged velocity, α is a universal constant, y is the distance coordinate measured from the surface and β is a constant depending on the roughness height ϵ. The assumptions under which the logarithmic velocity distribution law was obtained are given by Prandtl (1925). A detailed derivation of (12) can be found in Shames (1982).

It is important to note here that (12) was developed by Blasius for a flat plate (Shames 1982, pp. 322–323). However, in Shames' words 'experimental evidence indicates that we have the happy situation that not only is the relation above good in the expected region of two dimensional flow but also it is valid throughout the three dimensional symmetric flow in a pipe.... This relation shows excellent agreement with pipe flow data'. Consequently, it is a common practice to adopt correlations which were developed for boundary layers over flat plates as appropriate for pipe flows while considering y as the radial distance from the pipe wall and replacing half the distance between two parallel plates by the radius of the pipe R. Similarly, this procedure is also used in the opposite direction, i.e. expressions which were developed for pipe flows are used for flat plates by replacing the above-mentioned parameters. For example, Blasius (Shames 1982, p. 383) found that for a pipe flow

$$\tau_w = 0.0225\rho V_0^2\left(\frac{\nu}{V_0\delta}\right)^{\frac{1}{4}}.$$

Schultz-Grunow (Shames 1982, p. 383) later confirmed that this correlation is valid for flat plates also. The fact that the correlations for pipe flows and flows over flat plates are similar is known as the Blasius analogy. In the following the Blasius analogy is adopted; therefore, correlations which were originally developed for pipe flows are used for flat plates. A comparison between the experimental results of Nikuradse (1933) and (12) indicates that (i) for a large range of Reynolds numbers and roughness heights, $\alpha = 0.417$ (Shames 1982, p. 323); (ii) for a hydraulically smooth flow

$$\ln\beta = -2.2, \tag{13}$$

for the frictional transition flow

$$-2.2 \leqslant \ln\beta \leqslant 0.8, \tag{14}$$

and for the rough flow

$$\ln\beta = \frac{\epsilon V_*}{\nu} - 3.4. \tag{15}$$

Based on these values of α and β expressions for evaluating the friction coefficient f for flat plates were derived for each of the three flow zones. In order not to limit the present results to any specific flow zone a different analytical approach, outlined below, is taken in the present study.

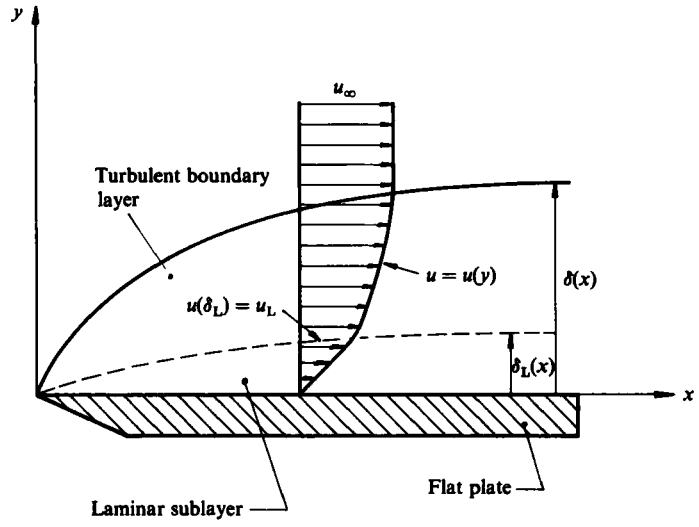

FIGURE 6. Schematical illustration of the laminar sublayer inside the turbulent boundary layer. The velocity profile inside the laminar sublayer is linearly changing from $u = 0$ at $y = 0$ to $u = u_L$ at $y = \delta_L$.

Inserting the boundary condition $u|_{y=\delta_L} = u_L$ (figure 6) into (12) yields

$$\frac{u_L}{V_*} = \frac{1}{\alpha}\left[\ln\frac{V_*\,\delta_L}{\nu} - \ln\beta\right]. \tag{16}$$

In the laminar sublayer the velocity changes linearly (Shames 1982, p. 325):

$$u_L = \frac{\tau_w}{\mu}\delta_L, \tag{17}$$

where τ_w is the shear stress on the surface. Inserting the relation $V_*^2 = \tau_w/\rho$ into (17) results in

$$\frac{u_L}{V_*} = \frac{V_*\,\delta_L}{\nu}. \tag{18}$$

Combining (16) and (18) yields

$$G = \frac{1}{\alpha}(\ln G - \ln\beta), \tag{19}$$

where G is defined as $G = V_*\,\delta_L/\nu$. For $\alpha = 0.417$ (19) reduces to

$$G = 2.398\,(\ln G - \ln\beta). \tag{20}$$

Since β depends solely on the roughness height ϵ, it is obvious from (20) that so does G, i.e. for any given value of ϵ, the value of G is independent of the flow properties. It is therefore suggested that G is called the 'roughness characterizer' and it should be noted that $G = V_*\,\delta_L/\nu$ is simply the common Reynolds number in the usual form applicable to the inner layer. The laminar-sublayer thickness δ_L is fundamental in the evaluation of G. Indeed, G does characterize the roughness effects, but should more properly be viewed as the ratio of the two lengthscales; δ_L and a viscous length ν/V_*.

For assessing the value of G associated with hydraulically smooth surfaces, Blasius'

ϵ [cm]	G
0	∞
< 0.00517	12.2468
0.01	6.3848
0.02	3.4845
0.08	1.0401
0.20	0.4750

TABLE 1. The dependence of G on ϵ in the range $1 < M_i < 2$

results can be used. Blasius (in Schlichting 1962) found that the friction coefficient for the case considered is given by

$$f = 0.3164\, Re_D^{-\frac{1}{4}}, \tag{21}$$

where $Re_D = u_{\mathrm{av}} D/\nu$. Equation (21), which is known as the Blasius equation, was derived for the following specific velocity profile:

$$\frac{\overline{u}}{u_0} = \left(\frac{y}{R}\right)^{\frac{1}{7}}. \tag{22}$$

For a general velocity profile,

$$\frac{\overline{u}}{u_0} = \left(\frac{y}{R}\right)^{n}, \tag{23}$$

(21) can be generalized to the following form:

$$f = C(n, G)\, Re^{-2n/n+1}. \tag{24}$$

In this relation the velocity power exponent n depends solely on the Reynolds number. Mazor (1984) showed that $C(n, G)$ has the following form:

$$C(n, G) = \{2^{5n+1}[(n+1)(n+2)]^2 G^{2(n-1)}\}^{1/n+1}. \tag{25}$$

Inserting $n = \frac{1}{7}$ into (25) and recalling that for this value of n $C(\frac{1}{7}, G) = 0.3164$ [see (21)] yields, for a hydraulically smooth surface, $G = 12.2468$. Using this value of G in (20) implies that for a hydraulically smooth surface $\ln\beta = -2.39$. This value of $\ln\beta$ is about 8% smaller than the value usually quoted in the literature [equation (13)].

The value of the roughness characterizer G for a frictional transition flow can be determined from (20). As mentioned earlier, for a frictional transition flow $-2.2 \leqslant \ln\beta \leqslant 0.8$ [equation (14)], thus by inserting $\ln\beta = 0.8$ into (20) the lower value of G for a frictional transition flow can be obtained. Following this procedure one obtains: for the hydraulically smooth flow $G = 12.2468$; for the frictional transition flow $0.5625 < G < 12.2468$; for the rough flow $0 < G < 0.5625$.

Mazor (1984) developed a method by which the roughness characterizer G can be calculated as a function of the surface roughness ϵ. The values of G for the values of ϵ used in the present study are shown in table 1. A fitted curve to these tabulated values yields

$$G = \frac{0.062}{\epsilon\,[\mathrm{cm}]} + 0.25. \tag{26}$$

It is worthwhile noting that this expression complies with the physical requirement that the value of the shear stress τ_w increases as the roughness height ϵ increases.

Note also that for a perfectly smooth surface ($\epsilon = 0$), (26) results in $G \to \infty$ and from (29) one obtains for this case $\tau_w \to 0$ as expected.

In the following, the boundary layer developing behind the reflection point of the regular reflection shown in figure 5(*a*) will be developed.

3.4. *The boundary-layer thickness*

The origin of the coordinate system is moving with the reflection point G along the wedge at a constant velocity $V_0 = u_i/\cos\theta_w$ (u_i is the incident shock wave velocity in the laboratory frame of reference and θ_w is the wedge angle, see figure 1). In this frame of reference the flow in state (0) is moving towards the incident shock wave (which is now stationary) with a velocity V_0 (the angle of incidence between this flow and the shock wave is $\phi_0 = 90° - \theta_w$). The wall, which in a laboratory frame of reference is at rest, is also moving now with the velocity $u_w = V_0$. The flow in state (2), which initially had an induced velocity $u_2(y)$, is now moving with the velocity $V_2(y) = [u_i - u_2(y)]/\cos\theta_w$. Therefore, in the considered frame of reference δ should be calculated for a flow velocity $V_2(y)$ over a moving flat plate having a velocity V_0 in the same direction as $V_2(y)$.

For turbulent incompressible boundary flows two different approaches are frequently used (both are semi-empirical): they are the mixing length of Prandtl and the von Kármán momentum integral (see Shames 1982, p. 368). Since similar semi-empirical approaches are not available for compressible, turbulent boundary-layer flows, it was suggested by Eckert (1954) and Mirels (1956) that the approaches proposed for incompresible flows should be adopted and adjusted to account for compressibility effects. A similar approach is adopted in the present study.

Prior to adjusting these approaches to the compressible case, the differences between the incompressible and the compressible cases should be understood. While in the former the velocity and thermal boundary layers can be considered separately, in the latter they are coupled because at high flow velocities the heat generated by friction and the temperature changes due to compressibility must be accounted for. Consequently, in the compressible case the following factors must be considered: (i) the Mach number; (ii) the Prandtl number; (iii) the viscosity dependence on temperature; and (iv) the heat transfer from the flow to the solid surface.

The major assumptions upon which the present model is developed are: (i) the gas behaves as a perfect gas; (ii) the flow is pseudo-steady and two-dimensional; (iii) the boundary layer is turbulent from $x = 0$ where x is measured from the reflection point G. This assumption is reasonable because (*a*) the *Re* number is very high; therefore, the boundary layer is laminar for a short distance only (Martin 1957), and (*b*) Schlichting (1962) showed that the surface roughness decreases the value of the critical Reynolds number for transition from laminar to turbulent flow; (iv) the gravitational forces can be neglected; (v) the pressure is constant throughout the entire field, i.e. $\partial P/\partial x = 0$ and $\partial P/\partial y = 0$; and (vi) Blasius' semi-empirical results for the wall shear stress τ_w in incompressible flows are applicable when the average temperature T_m is used.

In the following an expression for the wall shear stress in a compressible viscous flow over a moving rough flat plate is developed. The shear stress for an incompressible viscous flow over a rough stationary flat plate is (Mazor 1984)

$$\frac{\tau_w}{\rho_\infty} = u_\infty^2 G^{2(n-1)/n+1} Re_\delta^{-2n/n+1}, \tag{27}$$

where u_∞ and ρ_∞ are the flow velocity and density outside the boundary layer, G is the roughness characterizer $G = V_* \delta_L/\nu$, and

$$Re_\delta = \frac{u_\infty \delta}{\nu}.$$

Inserting $n = \frac{1}{7}$ and $G = 12.2468$ (the value calculated previously for hydraulically smooth surfaces) into (27) yields

$$\frac{\tau_w}{\rho_\infty} = 0.0233 u_\infty^2 Re^{-\frac{1}{4}}.$$

The fact that this is only 3.4 % larger than Blasius' expression for incompressible flows over a smooth plate, i.e.

$$\frac{\tau_w}{\rho_\infty} = 0.0225 u_\infty^2 Re^{-\frac{1}{4}},$$

clearly indicates the validity of (27).

In order to apply (27) to a compressible flow, the flow properties must be calculated for the average temperature inside the boundary layer, T_m. Consequently

$$\frac{\tau_w}{\rho_m} = u_\infty^2 G^{2(n-1)/n+1} \left(\frac{\nu_m}{u_\infty \delta}\right)^{2n/n+1}. \tag{28}$$

A similar approach was adopted by Tucker (1951), Eckert (1954), Bartz (1955) and Mirels (1956). Using $\nu_m = \mu_m/\rho_m$, $\nu_\infty = \mu_\infty/\rho_\infty$, $\rho_m = P_m/(RT_m)$, $\rho_\infty = P_\infty/(RT_\infty)$ and assumption (v), i.e. $P_\infty = P_m$ in (28) results in

$$\frac{\tau_w}{\rho_\infty} = u_\infty^2 G^{2(n-1)/n+1} Q \left(\frac{\nu_\infty}{u_\infty \delta}\right)^{2n/n+1}, \tag{29}$$

where

$$Q = \left(\frac{\mu_m}{\mu_\infty}\right)^{2n/n+1} \left(\frac{T_\infty}{T_m}\right)^{1-n/n+1}. \tag{30}$$

Equation (29) differs, as expected, from (27) by the term Q which accounts for the fact that the flow is compressible. In order to calculate Q, appropriate expressions for μ_m and T_m are required.

For non-polar diatomic gases, Mazor, Ben-Dor & Igra (1985) suggested

$$\frac{\mu}{\mu_0} = \left(\frac{T}{T_0}\right)^{0.64874};$$

therefore

$$\frac{\mu_m}{\mu_0} = \left(\frac{T_m}{T_0}\right)^{0.64874}. \tag{31}$$

Inserting this relation into (30) yields

$$Q = \left(\frac{T_\infty}{T_m}\right)^{1-2.2975n/n+1}. \tag{32}$$

Eckert (1954) showed that T_m can be approximated by

$$T_m = 0.5(T_w - T_\infty) + 0.22(T_r - T_\infty), \tag{33}$$

where T_w, T_∞ and T_r are the wall, the free-stream and the recovery temperatures respectively.

The recovery temperature T_r (which is equal to the wall temperature for the case when there is no heat transfer) can be calculated from (Schlichting 1962):

$$\frac{T_r}{T_\infty} = 1 + \left(\frac{u_w}{u_\infty} - 1\right)^2 \frac{u_\infty^2 Pr^{\frac{1}{2}}}{2T_\infty C_P}, \tag{34}$$

where u_w and u_∞ are the wall and free-stream velocities respectively, Pr is the Prandtl number (calculated at T_r) and C_P is the specific heat capacity at constant pressure (calculated at T_r).

Mirels (1956) showed that (33) and (34) can be combined to give

$$\frac{T_m}{T_\infty} = \frac{5.56\frac{u_w}{u_\infty} - 0.28\left[1 + \left(\frac{u_w}{u_\infty}\right)^2\right]}{6\frac{u_w}{u_\infty} - 1}. \tag{35}$$

Inserting (35) into (32) results in

$$Q = \left\{\frac{6\frac{u_w}{u_\infty} - 1}{5.56\frac{u_w}{u_\infty} - 0.28\left[1 + \left(\frac{u_w}{u_\infty}\right)^2\right]}\right\}^{1-2.2975n/n+1} \tag{36}$$

As previously mentioned, in the present case the frame of reference is attached to the reflection point G (see figure 1); thus $u_w = V_0$, $u_\infty = V_2$, $\rho_\infty = \rho_2$ and $\nu_\infty = \nu_2$. Inserting these terms into (29) and (36) results in

$$\frac{\tau_w}{\rho_2} = V_2^2 G^{2(n-1)/n+1} Q \left(\frac{\nu_2}{V_2 \delta}\right)^{2n/n+1} \tag{37}$$

and

$$Q = \left\{\frac{6\frac{V_0}{V_2} - 1}{5.56\frac{V_0}{V_2} - 0.28\left[1 + \left(\frac{V_0}{V_2}\right)^2\right]}\right\}^{1-2.2975n/n+1} \tag{38}$$

Equation (37) expresses the wall shear stress for a compressible flow over a rough flat plate. The compressibility is acounted for through Q and the roughness is accounted for through G. One additional correction is required in order to use (37) and (38) for the problem at hand; i.e. to account for the fact that in the present case the flat plate is not stationary. This can easily be done by replacing V_2 in (37), by the relative velocity between the flow and the surface, $V_2 - V_0$. Carrying out this transformation finally results in

$$\frac{\tau_w}{\rho_2} = (V_2 - V_0)^2 G^{2(n-1)/n+1} Q \left(\frac{\nu_2}{|V_2 - V_0| \delta}\right)^{2n/n+1}. \tag{39}$$

Inserting the velocity profile, (23), and the wall shear stress, (39), into von Kármán's momentum integral for the case of zero pressure gradient, i.e. $\partial P/\partial x = 0$ (see Schlichting 1962)

$$\tau_w = \frac{\mathrm{d}}{\mathrm{d}x} \int_0^\delta \rho[u^2 - (V_2 - V_0)\, u]\, \mathrm{d}y$$

results in

$$\frac{\delta}{x} = G^{2(n-1)/3n+1}\left(\frac{T_m}{T_2}\right)^{3.2975n/3n+1} Re_x^{-2n/3n+1}\left[\frac{(3n+1)(2n+1)}{n}\right]^{n+1/3n+1}, \tag{40}$$

where

$$Re_x = \frac{|V_2 - V_0|\, x}{\nu_2}.$$

Equation (40) describes the boundary-layer thickness for a compressible flow over a rough moving flat plate.

In the special case of an incompressible flow, $T_m/T_2 = 1$, over a smooth plate, $G = 12.2468$, when $n = \frac{1}{7}$, (40) reduces to

$$\frac{\delta}{x} = 0.3816\, Re_x^{-\frac{1}{5}}.$$

The expression found in the literature for this case is (see Schlichting 1962)

$$\frac{\delta}{x} = 0.376\, Re_x^{-\frac{1}{5}}.$$

The small difference between these two expressions (about 1.5%) again verifies the validity of the present approach.

3.5. *The boundary-layer displacement thickness* δ^*

The boundary-layer displacement thickness δ^* can be calculated from (Schlichting 1962)

$$\delta^* = \int_0^{\delta}\left(1 - \frac{\rho}{\rho_\infty}\frac{u}{u_\infty}\right)dy.$$

Inserting the velocity profile, (23), into the above equation and carrying out the integration, results in

$$\delta^* = \delta\frac{1}{n+1}\left(n+1-\frac{T_2}{T_m}\right). \tag{41}$$

Inserting (40) into (41) finally yields

$$\frac{\delta^*}{x} = CG^{2(n-1)/3n+1}\left(\frac{T_m}{T_2}\right)^{3.2975n/3n+1}\left(\frac{\nu_2}{|V_2 - V_0|\, x}\right)^{2n/3n+1}\left(n+1-\frac{T_2}{T_m}\right), \tag{42}$$

where

$$C = \frac{1}{n+1}\left[\frac{(3n+1)(2n+1)}{n}\right]^{n+1/3n+1} \tag{43}$$

Equation (42) describes the boundary-layer displacement thickness for a compressible flow over a rough surface of a flat plate which moves with the velocity V_0 relative to the free-stream velocity V_2. The plate roughness is accounted for by G and the compressibility of the flow by the term T_m/T_2; n, the velocity-profile exponent, depends solely on the Reynolds number. Checking for the well-known case of an incompressible flow over a hydraulically smooth plate, i.e. setting $T_m/T_2 = 1$, $G = 12.2468$ and using $n = \frac{1}{7}$ results in

$$\frac{\delta^*}{x} = 0.049\, Re_x^{-\frac{1}{5}}.$$

The appropriate expression in the literature is $\delta^*/x = 0.047\, Re_x^{-\frac{1}{5}}$. The small difference between these two expressions again verifies the validity of the approach of the present study.

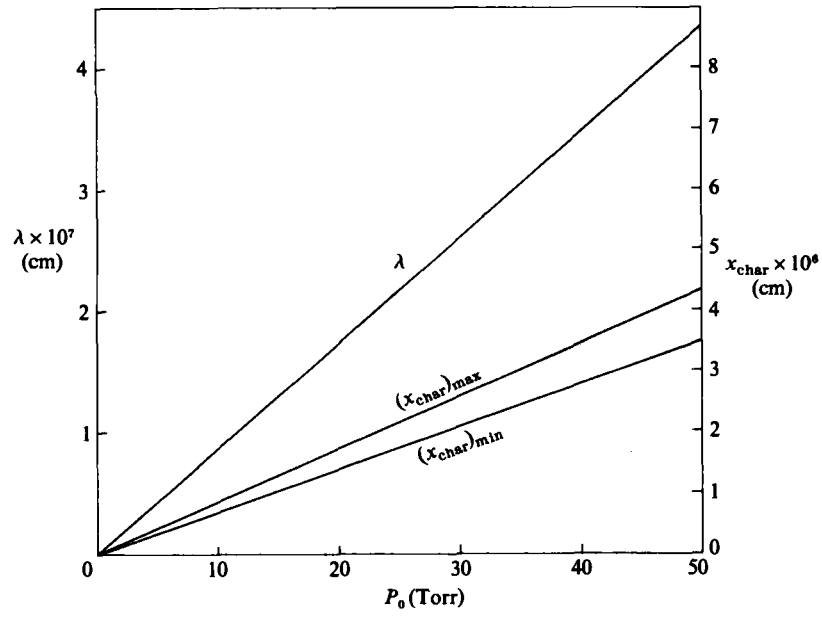

FIGURE 7. The dependence of the mean free path λ, $(x_{char})_{max}$ and $(x_{char})_{min}$ on the initial pressure P_0.

3.6. *The angle* γ

Once the displaced geometry is available, the question of how to determine the value of γ (equation (10)) arises. Intuitively, one might suggest the use of the slope of the displaced boundary at $x = 0$, i.e.

$$\gamma = \tan^{-1} \frac{d\delta^*}{dx}\bigg|_{x=0}.$$

However, inserting (42) into the last expression results in the non-physical value of $\gamma = 90°$. Consequently, it was suggested by Shirouzu & Glass (1982) that either

$$\gamma = \tan^{-1} \frac{d\delta^*}{dx}\bigg|_{x=x_{char}} \tag{44}$$

or

$$\gamma = \tan^{-1} \frac{\delta^*}{x}\bigg|_{x=x_{char}} \tag{45}$$

be used to calculate the value of γ. While their former expression defines γ as the slope of the displaced boundary at $x = x_{char}$, the latter defines γ as the average slope of the displaced boundary at $x = x_{char}$. The characteristic length x_{char} has also been discussed by Shirouzu & Glass (1982). As will be shown subsequently, the present study indicates that

$$8\lambda \leqslant x_{char} \leqslant 10\lambda, \tag{46}$$

where λ, the mean free path of the flow ahead of the incident shock wave can be obtained from

$$\lambda = \frac{P_0(\text{Torr})}{760} 6.6 \times 10^{-6} \text{ cm}. \tag{47}$$

The value of λ as a function of the initial pressure is illustrated in figure 7. The additional two lines in figure 7 stand for $(x_{\text{char}})_{\min} = 8\lambda$ and $(x_{\text{char}})_{\max} = 10\lambda$. Thus, figure 7 enables one to select the appropriate value of x_{char} for any given initial pressure P_0.

The foregoing discussion concludes the present model for calculating the RR $\rightleftarrows$ MR transition wedge angle over rough surfaces. The procedure for using the present model is as follows: calculate the value of λ using (47); calculate the value of x_{char} using (46); calculate the value of γ using (45) and (42); solve (2)–(10) for the above-obtained value of γ.

4. Evaluation of the experimental results and verification of the present model

A list of the experiments evaluated in the following discussion is given in table 2. The surface roughness ϵ (in cm), the incident-shock-wave Mach number M_1, and the value of the wedge angle θ_w^{tr} at which the RR $\rightleftarrows$ MR transition was observed are given in columns 2, 3 and 4 respectively. Column 5 lists the flow deflection angle θ_1 while passing through the incident shock wave. This information for each experiment was then used in the following way. Equations (2)–(10) were solved for each case. The value of γ was then varied using a Newton–Raphson iteration until the solution resulted in a value of θ_w^{tr} that agreed with the measured value (shown in column 4) to within 0.1 %. The obtained values of γ for all the experiments are shown in column 6 of table 2. The value of γ for experiment 16 is negative and hence this experiment should be considered as doubtful. Note that in figure 9 this experimental point lies above the detachment-criterion transition line, a fact sufficient to discard this point on the basis of a possible experimental error. In column 7 of table 2 the ratio γ/θ_1 is listed for all the remaining experimental points. The numerical results clearly indicate that for a given value of surface roughness ϵ, the value of γ/θ_1 is practically independent of the incident-shock-wave Mach number M_1. The only clear discrepancy in this seems to occur for the experiments with high incident-shock-wave Mach numbers, i.e. experiments 11, 21, 22, 31 and 41; the values of M_1 for these experiments are 3.99, 3.86, 3.70, 3.83 and 3.94 respectively.

A possible explanation for this behaviour might be the following. For incident shock waves in the range $M_1 < 2.068$, the shock-induced flow is subsonic, while for $M_1 > 2.068$, the shock-induced flow is supersonic. It is most likely that for large values of surface roughness the interaction between the induced supersonic flow introduces a mechanism that has not been considered in the foregoing model. It is also possible that at the higher value of M_1, real-gas effects such as vibration and dissociation which are ignored in the present model should be accounted for.

Thus, discarding the experiments with the high incident-shock-wave Mach numbers i.e. limiting the following discussion to the range $M_1 \leqslant 2$, and averaging the values of γ/θ_1 for every set of valid experiments with the same surface roughness, results in the values shown in table 3. The value of F_γ *vs.* ϵ are shown in figure 8 together with the following two fitted curves:

$$F_\gamma = -889.9\,\epsilon^2 + 48.7\,\epsilon - 0.078 \quad (0.005\,17 \leqslant \epsilon \leqslant 0.02 \text{ cm}), \tag{48a}$$

$$F_\gamma = -4.17\,\epsilon^2 + 3.08\,\epsilon + 0.48 \quad (0.02 \leqslant \epsilon \leqslant 0.2 \text{ cm}). \tag{48b}$$

For surface roughness smaller than $\epsilon = 0.005\,17$ cm, which is the value appropriate

Exp no. 1	ϵ (cm) 2	M_1 3	θ_w^{tr} [°] 4	θ_1 [°] 5	γ [°] 6	$F_\gamma = \frac{\gamma}{\theta_1}$ 7	$\frac{x_{char}}{\lambda}$ 8
1	$\leqslant 0.005$	2.48	47.58	26.99	4.32	0.16	9.6
2		2.14	48.63	24.34	3.16	0.13	9.1
3		1.76	49.11	20.23	1.82	0.09	8.6
4		1.52	47.62	16.62	1.99	0.12	9.1
5		1.36	45.52	13.38	2.01	0.15	9.0
6		1.26	43.35	10.35	1.66	0.16	9.2
7		1.17	39.56	7.16	1.29	0.18	9.5
8		1.10	34.27	4.29	1.07	0.25	9.2
9		1.04	25.85	1.38	0.21	0.15	9.0
11	0.01	1.99	44.80	32.76	8.85	0.27	8.5
12		1.87	45.56	22.79	7.75	0.34	9.0
13		1.45	43.59	15.90	6.04	0.38	9.7
14		1.22	40.69	9.02	2.98	0.33	8.8
15		1.10	35.16	4.50	1.22	0.27	8.7
16		1.02	25.40	0.80	−0.104	—	—
21	0.02	3.86	42.14	34.04	13.62	0.40	6.9
22		3.70	42.34	33.64	13.46	0.40	7.1
23		1.91	41.53	24.42	13.19	0.54	8.6
24		1.45	41.81	16.09	8.05	0.50	9.2
25		1.21	37.10	8.63	4.75	0.55	8.9
26		1.12	32.66	4.86	2.77	0.57	9.1
31	0.08	3.83	40.32	34.93	16.77	0.48	7.0
32		1.91	39.45	24.86	16.41	0.66	8.4
33		1.45	37.18	16.33	12.08	0.74	9.2
34		1.22	34.15	8.73	6.37	0.73	9.6
35		1.12	28.59	4.55	3.64	0.80	8.9
36		1.04	24.27	1.54	0.83	0.54	8.8
41	0.20	3.94	33.51	38.09	28.19	0.74	7.0
42		1.87	32.18	25.11	23.35	0.93	8.4
43		1.43	31.49	15.49	14.56	0.94	9.0
44		1.21	30.04	8.09	7.28	0.90	9.1
45		1.11	25.04	4.05	3.77	0.93	9.6

TABLE 2. Experimental data and evaluation

to a hydraulically smooth surface (see the Appendix), $F_\gamma = 0.15$. The value of $F_\gamma = 0$ results in the well known 'detachment criterion'.

Column 8 in table 2 was obtained using the following procedure. For each experiment, (45) was solved by changing the value of x_{char} until satisfactory agreement was obtained with the value of γ shown in column 6. Then x_{char} was divided by the mean free path λ. The obtained results indicate, as can be seen in table 2, that

$$8 \leqslant \frac{x_{char}}{\lambda} \leqslant 10.$$

It is of interest to note that the thickness of the incident shock wave i is about ten times the mean free path. Consequently, the above results indicate that

$$x_{char} \approx l_1,$$

ϵ [cm]	$F_\gamma = \dfrac{\gamma}{\theta_1}$
< 0.00517	0.15
0.01	0.32
0.02	0.54
0.08	0.70
0.20	0.93

TABLE 3. F_γ *vs.* ϵ for the range $1 < M_1 < 2$

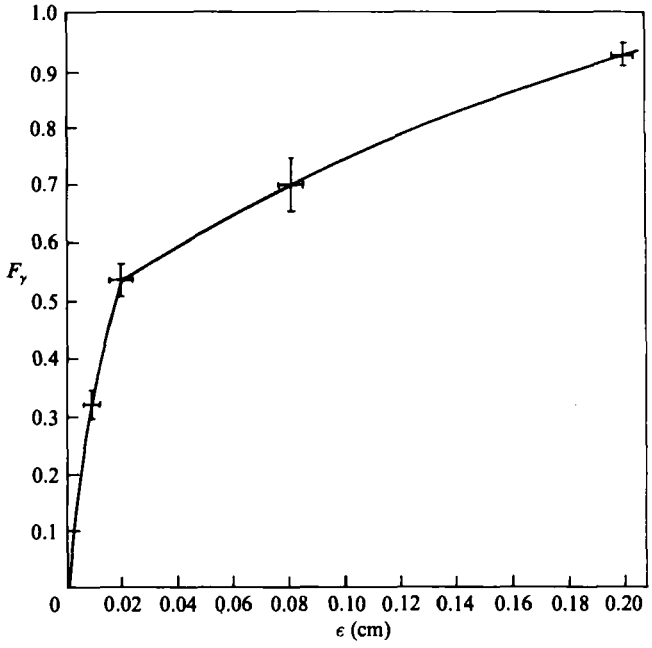

FIGURE 8. The present correlations of F_γ *vs.* ϵ for $0 < \epsilon \leqslant 0.2$ cm.

where l_i is the thickness of the incident shock wave. Thus, the incidence-shock-wave thickness is probably the characteristic length for the problem at hand.

The experimental data points (see details in table 2) are plotted in figure 9 in the (M_i, θ_w^{tr})-plane. The six solid curves in figure 9 are obtained from the solution of equations (2)–(10) using $F_\gamma = 0$, 0.15, 0.32, 0.54, 0.70, 0.93, which were found to be the average values of F_γ in the range $1 < M_1 \leqslant 2$ for $\epsilon = 0$, $0 < \epsilon < 0.00517$, and $\epsilon = 0.01$, 0.02, 0.08, 0.2 cm, respectively (see table 3 for details).

It is clear from figure 9 that the agreement between the prediction of the present model and the experimental results is good in the range $1 < M_1 \leqslant 2$. As the value of the incident-shock-wave Mach number increases, the agreement between the theory and the experiments becomes progressively worse.

5. Application of the present model

The foregoing discussion suggests two possible methods for analytically calculating the RR$\rightleftarrows$MR transition wedge angle over rough surfaces. The two methods are outlined in the following.

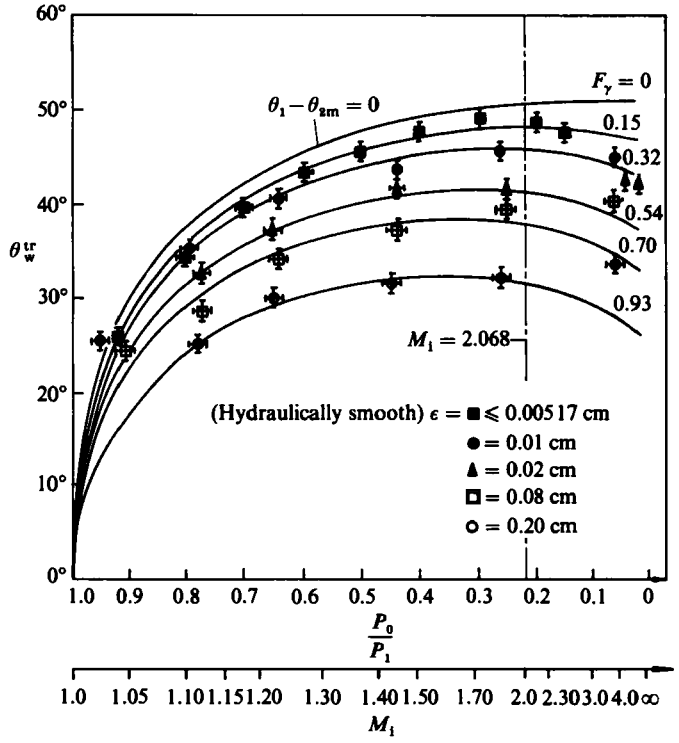

FIGURE 9. The experimental results as well as the prediction of the present model for the RR⇄MR transition over rough wedges.

(i) For a given set of initial conditions, i.e. initial pressure P_0, initial temperature T_0 and the incident-shock-wave Mach number M_1 one first has to calculate the flow properties of state (2) behind the reflected shock wave at 'detachment'. Then, using these flow properties together with the roughness size ϵ for the given experiment, the displacement angle γ can be calculated from (45) when $x_{\text{char}} = (8 \div 10)\lambda$. Once γ is obtained, (2)–(10) can be solved to obtain the RR⇄MR transition wedge angle for the given experiment.

(ii) Unlike the previous method, this relies more heavily on empirical considerations. However, it is much easier to use, and much faster in obtaining practical results. Using the given surface roughness ϵ, one can calculate the value of F_γ from the appropriate correlation (48*a*) or (48*b*). Then (2)–(10) can be solved to obtain the RR⇄MR transition wedge angle.

In order to provide an additional verification of the suggested models for calculating the RR⇄MR transition wedge angle for rough surfaces, additional experiments with $\epsilon = 0.04$ cm were performed. The recorded experimental data points are shown in figure 10.

Using $\epsilon = 0.04$ and (48*b*), one obtains $F_\gamma = 0.60$. The RR⇄MR transition line as obtained form the solution of (2)–(10) with $F_\gamma = 0.60$, as well as the 'detachment' transition line, i.e. $F_\gamma = 0$, are both shown in figure 10. It is clearly seen that the predictions of the present model are in fairly good agreement with the experimental results in the range $1 < M_1 < 2$. The poor agreement in the range $M_1 > 2$, which has already been pointed out, can again be seen.

The two dashed lines were obtained using (45) with $x_{\text{char}} = 8\lambda$ and 10λ. Note that in this case, two values of γ were obtained for each experiment – one appropriate to

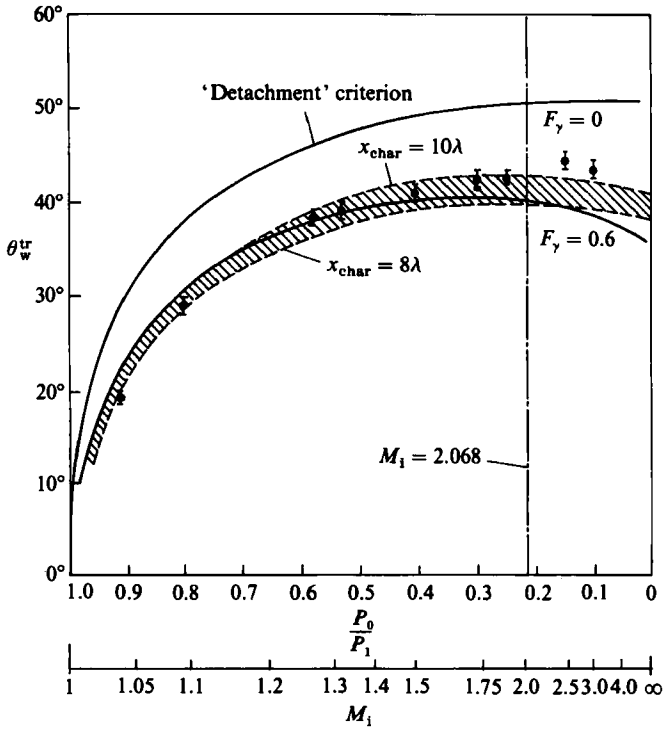

FIGURE 10. Experimental results of the RR ⇄ MR transition over a rough wedge with $\epsilon = 0.04$ cm and the predictions of the present models, i.e. $F_\gamma = 0.6$ and the region of possible transition bounded by $8\lambda \div 10\lambda$, where λ is the mean free path of the flow ahead of the incident shock wave.

$x_{char} = 8\lambda$ and the other to $x_{char} = 10\lambda$. The two dashed lines represent the best second-order fit for the obtained value of γ. The shaded area between these two dashed lines indicates the region in which the RR ⇄ MR transition should occur for a surface with $\epsilon = 0.04$ cm. Unlike these two dashed lines the solid curves were calculated continuously for the entire range of incident-shock-wave Mach numbers.

6. Conclusions

A detailed investigation of our experimental results for the transition from regular to Mach reflection over rough surfaces enabled us to develop a model for predicting the RR ⇄ MR transition wedge angle.

The model is based on displacing the boundary surface according to the mass displacement thickness and requiring that the flow behind the reflection point must adjust to the displaced surface. In order to obtain the displaced surface, an expression for the turbulent boundary-layer thickness of a compressible flow over a rough surface was developed. To the best of our knowledge such an expression has never been presented before.

Using the expression for the boundary-layer thickness an appropriate expression for the mass displacement thickness δ^* was derived. It was shown that the flow behind the reflection point must be parallel to the average slope of the displaced surface, i.e. $\tan^{-1}\delta^*/x$, at a characteristic distance $x = x_{char}$, which was found to be of the order of eight to ten mean free paths. This value is also comparable to the incident shock-wave thickness.

It was also shown that the present model is limited to the range $1 < M_1 < 2$. Two possible reasons for this limitation were presented. One argues that the value of $M_1 = 2.068$ might be critical since below it the shock-induced flow is subsonic and above it, it is supersonic. The other reason might arise from the neglect of the real-gas effects although, as shown by Ben-Dor & Glass (1979), vibrational relaxation starts at about $M_1 = 2$. It is also of interest to note that Reichenbach (1985) in a recent paper has conducted experiments over rough surfaces where the roughness shape was different from the 'saw-tooth' shape used in our experimental study. In spite of the different roughness shape, almost identical transition wedge angles were obtained for identical roughness heights.

The financial assistance received from the US Army under Grant No. DAJA-45-83-C-0046 and from the Wolf Foundation are gratefully acknowledged.

Appendix. The height of the surface roughness for a hydraulically smooth wedge

In the following, the maximum surface-roughness height for which the surface can still be regarded as hydraulically smooth is calculated. The calculation is based on the assumptions given in the paper.

The roughness characterizer G was defined (equation 19) as

$$G = \frac{V_* \delta_L}{\nu}, \tag{A 1}$$

where V_*, the shear velocity, is

$$V_* = (\tau_w/\rho)^{\frac{1}{2}}. \tag{A 2}$$

Inserting the expression for τ_w (equation 39) into (A 2) results in

$$V_* = (V_2 - V_0)\, G^{n-1/n+1} \left(\frac{\nu_2}{\delta |V_2 - V_0|}\right)^{n/n+1} Q^{\frac{1}{2}}. \tag{A 3}$$

Inserting (A 3) into (A 1) and rearranging, yields

$$\delta_L = G^{2/n+1} \left(\frac{\nu_2}{|V_2 - V_0|}\right)^{1/n+1} \delta^{n/n+1} Q^{-\frac{1}{2}}. \tag{A 4}$$

In (A 4) the laminar sublayer thickness δ_L is given for a compressible turbulent flow over a non-stationary rough surface. The compressibility of the gas is accounted for through Q (see (36)) and the roughness is accounted for through G. The boundary-layer thickness δ is given in (40).

For a typical incident-shock-wave Mach number in the range $1 < M_1 < 2$, i.e. $M_1 = 1.5$, and for the value of G appropriate for a hydraulically smooth surface, i.e. $G = 12.2468$, as well as $n = \frac{1}{5}$, which is suggested for shock-tube experiments in this range of incident-shock-wave Mach numbers by Martin (1957) and Glass & Hall (1959), one obtains

$$\delta_L = 0.00517 \text{ cm}.$$

As mentioned earlier, the surface can be considered as hydraulically smooth as long as $\epsilon < \delta_L$. Thus, the maximum surface roughness for which the surface can be regarded as hydraulically smooth is

$$\epsilon_{max} = 0.00517 \text{ cm}.$$

It should be noted that this value is based on typical parameters at the centre of the incident-shock-wave Mach-number range $1 < M_i < 2$. For values smaller or greater than $M_i = 1.5$, the value of ϵ_{max} might change slightly.

REFERENCES

Bartz, D. R. 1955 *Trans. ASME* **77**, 1235.

Ben-Dor, G. 1978 *UTIAS Rep.* 232. University of Toronto, Toronto, Canada.

Ben-Dor, G. & Glass, I. I. 1979 *J. Fluid Mech.* **92**, 459.

Bleakney, W. & Taub, A. H. 1949 *Rev. Mod. Phys.* **21**, 584.

Eckert, E. R. G. 1954 *Tech. Rep.* 54–70. Aero. Res. Lab., Wright Air Dev. Ctr., Wright Patterson A.F. Base, USA.

Fletcher, C. H. 1950 *Tech. Rep.* II-4. Dept. of Physics, Princeton University, NJ, USA.

Glass, I. I. & Hall, J. G. 1959 *Handbook of Supersonic Aerodynamics.* Sec. 18, *Shock Tubes*, NAVORD Rep. 1488, Vol. 6.

Henderson, L. F. & Lozzi, A. 1975 *J. Fluid Mech.* **68**, 139.

Henderson, L. F. & Woolmington, J. P. 1983 *Shock Tubes and Waves* (ed. R. D. Archer & B. E. Milton), p. 160. New South Wales University Press.

Hornung, H. G. & Taylor, J. R. 1982 *J. Fluid Mech.* **123**, 145.

Hopf, L. 1923 *Z. angew. Math. Mech.* **3**, 329.

Law, C. K. 1970 *UTIAS TN* No. 150. University of Toronto, Toronto, Canada.

Martin, W. A. 1957 *UTIAS Rep.* 47. University of Toronto, Toronto, Canada.

Mazor, G. 1984 Surface roughness effect on the transition from regular to Mach reflection in pseudo-steady flows. M.Sc. thesis. Department of Mechanical Engineering, Ben-Gurion University of the Negev, Beer Sheva, Israel.

Mazor, G., Ben-Dor, G. & Igra, O. 1985 *AIAA J.* **23**, 636.

Mirels, H. 1956 *NACA TN* 3712.

Neumann, J. von 1943 *Explosive Res. Rep.* 12. Department of the Navy, Bureau of Ordnance, Washington, DC, USA.

Neumann, J. von 1963 *Collected Works*, Vol. 6. Pergamon.

Nikuradse, J. 1933 *Forschungsheft* **361**.

Prandtl, L. 1925 *Z. angew. Math. Mech.* **5**, 136, Proc. 2nd Intl Cong. Appl. Mech., Zurich (1926).

Reichenbach, H. 1985 *The 5th Mach Reflection Symp., Menlo Park, California, USA, 22–25 July.*

Schlichting, H. 1962 *Boundary Layer Theory*, 4th edn, pp. 475–563. McGraw-Hill.

Shames, I. H. 1982 *Mechanics of Fluids*, 2nd edn, pp. 257–426. McGraw-Hill.

Shirouzu, M. & Glass, I. I. 1982 *UTIAS Rep.* 264, University of Toronto, Toronto, Canada.

Smith, L. G. 1945 *OSRD Rep.* 6271 or (*NORC Rep.* A2350.)

Takayama, K., Ben-Dor, G. & Gotoh, J. 1981 *AIAA J.* **19**, 1238.

Taub, A. H. 1947 *Rev. Mod. Phys.* **21**, 51.

Tucker, M. 1951 *NACA TN* 2337.

White, D. R. 1951 *Tech. Rep.* II-10, Department of Physics, Princeton University, NJ, USA.